Supplementary Data

Supplementary Methods

Atrial tissue collection and processing

Before the institution of cardiopulmonary bypass, a purse-string suture was made around the atrial appendage for insertion of the venous cannula. A sample of the right atrial appendage (RAA) was then resected and immediately rinsed in ice-cold Buffer X. From the endocardial side of the RAA, a piece of atrial myocardium was dissected and a portion of this myocardial tissue was immediately frozen in liquid N_2 for biochemical analysis of RNA, proteins, and lipids. A portion of fresh atrial myocardium was kept in Buffer X (in m*M*: 7.23 K_2EGTA, 2.77 CaK_2EGTA, 20 Imidazole, 20 Taurine, 5.7 ATP, 14.3 PCr, 6.56 $MgCl_2 \cdot 6H_2O$, 50 MES; pH 7.4) and transferred to the laboratory to be used for the preparation of permeabilized myofibers bundles (PmFBs) and analysis of mitochondrial function. Another portion of this fresh tissue was placed in hypotonic buffer (in m*M*: 10 HEPES, pH 7.5; 40 NaF; 0.01 Na_2MoO_4; 0.1 EDTA, 1 β-glycerophosphate; 1 Na_3VO_4) and protease inhibitor cocktail (Sigma), and transferred to laboratory for the preparation of nuclear extracts as described next. Laboratory personnel involved in performing lipid analysis and other biochemistry were blinded to the treatment groups.

Fatty acid analysis of whole blood and myocardial tissue

Myocardial tissue was disrupted and pulverized using a Dounce homogenizer, and fatty acids were then extracted from this tissue, and whole blood, with HPLC grade organic solvents using the Folch method (13). Extracted fatty acids were then methylated using boron trifluoride in methanol (Sigma Chemical Co) for 90 min at 100°C. Methyl esters were extracted into hexane and separated by capillary GC (Shimadzu 2010; Shimadzu Scientific Instruments) with a Restek RT-2560 column. Data were analyzed by summing the identified peaks, and each peak area (representing individual fatty acids) is shown as the percentage of total peak area. Peaks were identified with several standards from Restek and Nu-Chek Prep. Data were analyzed using GCsolution (Shimadzu Scientific Instruments).

Permeabilized atrial myofiber preparation

This technique has been previously described in detail, and has been adapted for application in human cardiac muscle and for specific measurements made in this study (2, 4). After RAA tissue harvest, muscle was dissected from the endocardial side of the RAA sample and placed in ice-cold Buffer X, containing (in m*M*: 7.23 K_2EGTA, 2.77 CaK_2EGTA, 20 Imidazole, 20 Taurine, 5.7 ATP, 14.3 PCr, 6.56 $MgCl_2 \cdot 6H_2O$, 50 MES; pH 7.4). Portions of the muscle was then cut into small strips $\sim$4–6 mm long $\times$ 2–3 mm wide, placed in a solution of Buffer X containing 3 mg/ml collagenase Type I (Sigma-Aldrich), and incubated for 30–45 min at 4°C. Fiber bundles were then carefully trimmed of vascular and connective tissue, separated along their longitudinal axis, and permeabilized for 30 min in Buffer X + 50 μg/ml saponin at 4°C. Only 30 μg/ml saponin was used if the patient was a woman, for reasons previously described (17). After that, PmFBs were washed in ice-cold Buffer Z containing (in m*M*): 110 K-MES, 35 KCl, 1 EGTA, 5 K_2HPO_2, 3 $MgCl_2$-$6H_2O$, and 5 mg/ml BSA (pH 7.4, 295 mOsm) and remained in Buffer Z on a rotator at 4°C until analysis ($<$2 h). In a previous report, we had described how human PmFBs exhibit a very strong Ca^{2+}-independent contraction that is temperature sensitive and can occur even at 4°C with prolonged incubation (24); therefore, 20 μM Blebbistatin (Sigma-Aldrich) was added to the wash buffer, in addition to the respiration medium (Buffer Z) during experiments, to prevent the Ca^{2+}-independent contraction.

Measurement of mitochondrial ATP generation, O_2 consumption, and H_2O_2 emission in cardiac PmFBs

All mitochondrial measurements in this study were performed at 30°C. Mitochondrial O_2 consumption was measured using the O_2K Oxygraph system (Oroboros Instruments) in Buffer Z containing 20 m*M* creatine monohydrate (Sigma-Aldrich) and 20 μM Blebbistatin. O_2 consumption was supported by 125 μM palmitoyl-L-carnitine/2 m*M* malate, or 5 m*M* pyruvate/2 m*M* malate, as indicated in the Figure legends. Measurements of mitochondrial ATP generation were obtained using a customized tandem oxifluorometer approach that was developed and validated in our laboratory (4), by coupling ATP hydrolysis to NADPH generation.

The rate of ATP production was then continuously assessed alongside the O_2 consumption in real time, by monitoring the increasing fluorescence in the respiration chamber coming from NADPH (340ex/460em) with a spectrofluorometer (Photon Technology Instruments), similar to a method described elsewhere (15). To maintain this reaction, 2.5 U/ml of glucose-6-phosphate dehydrogenase G6PDH (Roche), 2.5 U/ml yeast hexokinase (Roche), 5 m*M* nicotinamide adenine dinucleotide phosphate (NADP+) (Sigma-Aldrich), and 5 m*M* D-glucose (Sigma-Aldrich) were added to the assay media. P_1,P_5-Di(Adenosine-5′)Pentaphosphate (Ap5A) (Sigma-Aldrich) was included in respiration medium to inhibit adenylate kinase and to ensure that ATP production was solely due to the mitochondrial electron transport system (mito-ETS). An absolute amount of ATP generated across a given time frame was then calculated using a standard curve of fixed concentrations of ATP added to the saturating amounts of hexokinase, glucose, G6PDH, and NADP+. The rate of H_2O_2 coming from mito-ETS supported by 125 μM palmitoyl-L-carnitine, 5 m*M* glutamate, and 5 m*M* succinate oxidation was determined in PmFB's with 100 μM ADP, 5 m*M* glucose, and 1 U/ml hexokinase present to maintain the mitochondria in a permanent, submaximal phosphorylating state (*i.e.*, most physiological) (2, 4). The mitochondrial H_2O_2 emission rate (mito-JH_2O_2) was determined in real time using a spectrofluorometer (Photon Technology Instruments), by continuous monitoring of Amplex Red oxidation in the presence of horseradish peroxidase (1 U/ml) and superoxide dismutase (25 U/ml). To determine the contribution

of Thioredoxin Reductase-2 (TxnRd2) toward preserving the mitochondrial matrix redox state, mito-JH_2O_2 experiments were performed in both the absence and presence of the TxnRd2-specific inhibitor Auranofin (1 μM), as previously described by our group (12) and others (30).

RNA extraction and qRT-PCR measurement of gene expression in atrial tissue

Atrial samples frozen in liquid N_2 were homogenized in a glass grinder (Kimble Chase) and then subjected to brief proteinase K treatment (55°C, 10 min). Total mRNA was then extracted in RNeasy columns according to the manufacturer's instructions (Qiagen, Inc.). Reverse transcription and relative changes in mRNA of target genes were determined by fluorescence-based quantitative real-time PCR using SsoAdvanced™ SYBR® Green Supermix (BioRad Laboratories). All primer sequences used in this study are listed in Supplementary Table S1. The mRNA for 18S ribosome was used as a normalizing control.

Preparation of myocardial whole tissue and nuclear extracts, and immunoblot analysis

For whole tissue protein preparation, myocardial samples frozen in liquid N_2 were homogenized in ice-cold 10×(wt./vol) TEE buffer containing (in m*M*: 10 Tris base, 1 EDTA, and 1 EGTA), and 0.5% Tween-20, using a glass grinder (Kimble Chase). After 5 min of incubation on ice, homogenates were spun at 10,000 rpm for 10 min to pellet debris, and supernatants were retained for protein and enzyme analysis. Nuclear extract preparations were performed using fresh portions of atrial tissue immediately after dissection from the patient, according to the method described by Deryckere and Gannon (10). Briefly, after the removal of connective tissue, the fresh myocardial tissue was placed in ice-cold hypotonic buffer [10 m*M* HEPES, pH 7.5; 40 m*M* NaF; 10 μM Na_2MoO_4; 0.1 m*M* EDTA, 1 m*M* β-glycerophosphate; 1 m*M* Na_3VO_4, and protease inhibitor cocktail (Sigma)] and transferred to the laboratory. Tissue was then minced very fine, placed back into ice-cold hypotonic buffer, pulverized in a dounce homogenizer for 10–12 strokes, and incubated on ice for 15 min. The sample was then centrifuged at 300 *g* for 10 min, and the supernatant was retained as a cytosolic fraction. The pellet was then resuspended in ice-cold hypotonic buffer and again incubated for 15 min on ice. Nonidet P-40 was added at 0.1× the sample volume and centrifuged at 14,000 *g* for 30 s. This supernatant was also retained as the cytosolic fraction, and the pellet was resuspended in nuclear extraction buffer [10 m*M* HEPES, pH 7.9; 0.1 m*M* EDTA; 3 m*M* $MgCl_2$; 420 m*M* $NaCl_2$; 10% glycerol (v/v)], vortexed at full speed for 30 s, and then incubated for 15 min at 4°C with rocking. This step was repeated. The sample was then centrifuged at 14,000 *g* for 10 min at 4°C, and the supernatant was retained as the nuclear fraction.

Proteins in these extracts were subjected to SDS-PAGE, transferred to PVDF membrane, and probed *via* immunoblot procedure using the following antibodies: anti-PPARγ (Cell Signaling, Inc.), anti-NFκB p65 (Abcam, Inc.), anti-Nrf2 [EP1808Y]–Carboxyterminal end (Abcam), anti-TATA binding protein for nuclear loading control (Abcam), anti-Thioredoxin Reductase-2 (Pierce Biotechnology), anti-COX

SUPPLEMENTARY TABLE S1. PRIMER SEQUENCES USED FOR QRT-PCR.

Target	*Sense*	*Antisense*	*Reference*
18s	cag cca ccc gag att gag ca	tag tag cga cgg gcg gtg tg	(26)
TFAM	agc tca tgg act tct gcc agc a	cct gcc tcc ata ata taa gga aac aag agt	(11)
Catalase	gac tga cca ggg cat caa aaa	cgg atg cca tag tca gga tct t	(28)
PPARα	cca gta ttt agg aag ctg tcc	tga aag cgt gtc cgt gat	(14)
CPT1B	act gct aca aca ggt ggt t	tct gca ttg aga ccc aac tg	(14)
CD36	gtt gcc ata atc gac ac	gca gtg act ttc cca ata gg	(14)
LCAD	ctt cca cag gaa agg ctg tt	ctg cta att tat gtt gca ctg	(14)
HFABP	cag cag atg aca gga agg	ccg att ggc aga gta gta g	(14)
NRF1	cca gtt tag tgg gtg gta gg	cgg gag ctt tca aga cat tc	(33)
UCP2	tct aca atg ggc tgg tgg c	tgt atc tcg tct tga cca c	(22)
CRP	tcg tat gcc acc aag aga caa gac a	aac act tcg cct tgc act tca tac t	(21)
GPx1	tgt gcc cct acg cag gta ca	ccc ccg aga cag cag ca	(25)
GPx4	cga tac gct gag tgt ggt ttg c	cat ttc cca gga tgc cct tg	(8)
TNFα	atc aat cgg ccc gac tat ctc	gca atg atc cca aag tag acc tg	(18)
IL-1β	aaa caa cct gaa cct tcc aaa ga	gca agt ctc ctc att gaa tcc a	(18)
iNOS	ggt ttc ccc cag ttc ctc a	tct cca ttg ccc cag ttt tt	(27)
GSTA-1	gac tcc agt ctt atc tcc agc ttc c	gac tcc agt ctt atc tcc agc ttc c	(20)
HO-1	tgc ggt gca gct ctt ctg	gca acc cga cag cat gc	(29)
TxnRd2	ctg cat ttc ctt ggc ccc	gat acc cac ggt ccg cat c	(32)
GR	atc ccc ggt gcc agc tta gg	agc aat gta acc tgc acc aac aa	(9)
GCLC	gtt ctt gaa act ctg caa gag aag	atg gag atg gtg tat tct tgt cc	(7)
NQO1	aag ccc aga cca act tct	att tga att cgg gcg tct gct g	(25)

Primer sequences for target genes analyzed in this study. The source of the sequence from other literature is indicated. TFAM, mitochondrial transcription factor A; CPT1B, carnitine palmitoyl transferase-1B; LCAD, very long-chain acyl CoA dehydrogenase; HFABP, human fatty acid binding protein; NRF1, nuclear respiratory factor 1; UCP2, uncoupling protein 2; CRP, C-reactive protein; GPx1, glutathione peroxidase 1; GPx4, glutathione peroxidase 4; TNFα, tumor necrosis factor α; IL1β, interleukin-1β; iNOS; inducible nitric oxide synthase; GST-A1, glutathione -s-transferase A-1; HO-1, heme oxygenase-1; TxnRd2, thioredoxin reductase-2; GR, glutathione reductase; GCLC, γ-Glutamylcysteine ligase catalytic subunit; NQO1, NAD(P)H:quinone oxidoreductase 1.

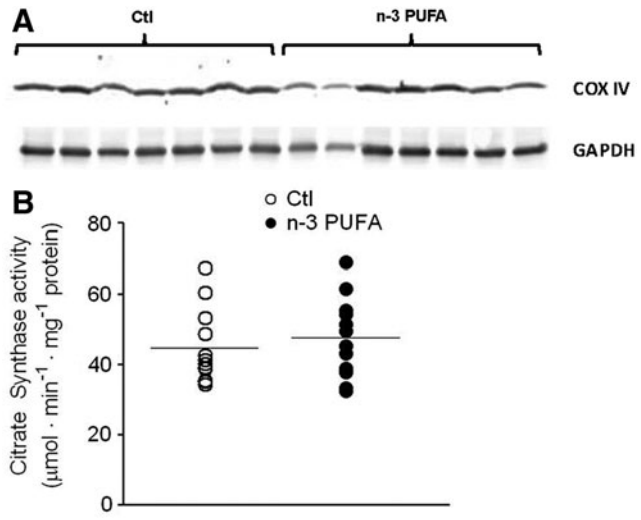

SUPPLEMENTARY FIG. S1. Biochemical markers of mitochondrial content in atrial myocardium. Two independent biochemical markers of mitochondrial content in atrial myocardium are shown for both treatment groups. In **(A)** is a representative immunoblot showing total COX IV protein in tissue homogenate from both treatment groups, along with **(B)** citrate synthase activity in both groups. $N = 7–12$ for each group.

IV (Abcam), anti-α Tubulin (Abcam), and anti-GAPDH (Abcam).

Redox enzyme activity in atrial tissue

All enzyme activity and glutathione assays were performed on the same day as the protein extraction. We have empirically determined that human cardiac glutathione and enzyme activity should be assessed immediately in protein extractions to obtain consistent and reproducible results, and that freezing samples or keeping them at 4°C overnight will cause a dramatic loss of content and activity. Total glutathione measurements were performed as previously described (3, 5) using a modified Tietze method (31). GR activity in myocardial tissue was measured in TEE buffer containing 1 m*M* GSSG and 0.5 m*M* NADPH, where activity was calculated from the linear decrease in NADPH absorbance with time (6). Glutathione peroxidase (GPx) activity was determined in TEE buffer containing 1 m*M* GSH, 100 mU/ml of purified GR enzyme, and 0.5 m*M* NADPH. The reaction was initiated with a nominal amount of tert-Butyl-Hydroperoxide, and the activity of GPx was calculated from the linear decrease in NADPH absorbance with time (23). MAO activity was determined in real time by continuous monitoring of clorgyline-sensitive H_2O_2 production supported by 1 m*M* Tyramine as previously described (16).

Measurement of protein modification by PUFA-derived aldehydes in atrial tissue

The absolute amount of n-6 PUFA-derived HNE-adducts and n-3 PUFA-derived HHE-modified protein adducts in atrial tissue was determined by a quantitative ELISA approach that was developed and validated in our lab (12, 19). A standard curve of aldehyde-modified protein adducts was first established by incubating saturating amounts of HNE or HHE (Cayman Chemical) with predetermined concentrations of BSA. After an overnight incubation at 37°C, aldehyde-BSA adducts were added to an Immunolon-coated 96-well assay plate (Fisher Scientific) along with diluted cardiac protein. Samples were incubated overnight at 4°C, subsequently washed with PBS + 0.05% Tween-20, and blocked for 2 h with NB4025 (NOF America). Samples were then incubated with anti-HNE-His antibody (1 μg/ml in PBS; Percipio Biosciences), or anti-HHE-His antibody (1 μg/ml in PBS; Genox) for 2 h at 37°C. Samples were washed with PBS + 0.05% Tween-20 and incubated with secondary antibody for 2 h at room temperature (goat anti-mouse HRP; Bio-Rad). After this incubation, samples were washed as earlier and incubated with TMBZ for 20 min at room temperature. The reaction was quenched with 1 *M* sulfuric acid, and the absorbance of the samples at 450 nm was determined. Total quantities of HNE- and HHE-modified proteins in each group were determined using a standard curve of aldehyde-modified BSA, and expressed in absolute amount as mmol/g protein.

Statistical analysis

Based on our previous work studying mitochondrial function and gene expression in atrial myocardium from diseased humans (1, 2, 4), and from our recently published work with n-3 PUFA diet in animal models (5), we estimated that a minimum of 12 patients in each group would be needed to detect an n-3 PUFA treatment effect of 20% or more (using anti-inflammatory gene expression as an outcome variable) at the $\alpha = 0.05$ level of significance with at least 80% power. Statistical analysis and graphics were prepared using GraphPad Prism 5 (GraphPad Prism). Data are presented as mean ± SD, with most graphical representation of data showing raw data points for every patient, along with the mean. Statistical significance of group comparisons for categorical variables was determined using Fisher's Exact, while paired and unpaired Students *t*-tests were performed to compare within-group and between-group differences, respectively. Statistical significance was defined as $p \leq 0.05$.

Supplementary References

1. Anderson EJ CW, Lehr EJ, Stevens LM, Ferguson TB, and Rodriguez E. Left atrium mitochondria of NYHA class I patients with severe mitral valve regurgitation display alterations in H_2O_2 and Ca^{2+} handling: early translational efforts to define role of mitochondria in human cardiac disease. *Circulation* 122: A16837, 2010.
2. Anderson EJ, Kypson AP, Rodriguez E, Anderson CA, Lehr EJ, and Neufer PD. Substrate-specific derangements in mitochondrial metabolism and redox balance in the atrium of the type 2 diabetic human heart. *J Am Coll Cardiol* 54: 1891–1898, 2009.
3. Anderson EJ, Lustig ME, Boyle KE, Woodlief TL, Kane DA, Lin CT, Price JW, 3rd, Kang L, Rabinovitch PS, Szeto HH, Houmard JA, Cortright RN, Wasserman DH, and Neufer PD. Mitochondrial H2O2 emission and cellular redox state link excess fat intake to insulin

resistance in both rodents and humans. *J Clin Invest* 119: 573–581, 2009.
4. Anderson EJ, Rodriguez E, Anderson CA, Thayne K, Chitwood WR, and Kypson AP. Increased propensity for cell death in diabetic human heart is mediated by mitochondrial-dependent pathways. *Am J Physiol Heart Circ Physiol* 300: H118–H124, 2011.
5. Anderson EJ, Thayne K, Harris M, Carraway K, and Shaikh SR. Aldehyde stress and up-regulation of Nrf2-mediated antioxidant systems accompany functional adaptations in cardiac mitochondria from mice fed n-3 polyunsaturated fatty acids. *Biochem J* 441: 359–366, 2012.
6. Carlberg I and Mannervik B. Glutathione reductase. *Methods Enzymol* 113: 484–490, 1985.
7. Chen CC, Chen HL, Hsieh CW, Yang YL, and Wung BS. Upregulation of NF-E2-related factor-2-dependent glutathione by carnosol provokes a cytoprotective response and enhances cell survival. *Acta Pharmacol Sin* 32: 62–69, 2011.
8. Cole-Ezea P, Swan D, Shanley D, and Hesketh J. Glutathione peroxidase 4 has a major role in protecting mitochondria from oxidative damage and maintaining oxidative phosphorylation complexes in gut epithelial cells. *Free Radic Biol Med* 53: 488–497, 2012.
9. Corrales RM, Galarreta D, Herreras J, Calonge M, and Chaves F. Antioxidant enzyme mRNA expression in conjunctival epithelium of healthy human subjects. *Can J Ophthalmol* 46: 35–39, 2011.
10. Deryckere F and Gannon F. A one-hour minipreparation technique for extraction of DNA-binding proteins from animal tissues. *Biotechniques* 16: 405, 1994.
11. Fabricius MH, Wilms LK, Larsen J, Pedersen PL, Anthonsen S, and Kvetny J. Measure of expression of mitochondrial related genes in human mononuclear blood cells, adipose white tissue and smooth muscle cells. *Clin Chim Acta* 411: 749–753, 2010.
12. Fisher-Wellman KH, Mattox TA, Thayne K, Katunga LA, La Favor JD, Neufer PD, Hickner RC, Wingard CJ, and Anderson EJ. Novel role for thioredoxin reductase-2 in mitochondrial redox adaptations to obesogenic diet and exercise in heart and skeletal muscle. *J Physiol* 591: 3471–3486, 2013.
13. Folch J, Lees M, and Sloane Stanley GH. A simple method for the isolation and purification of total lipides from animal tissues. *J Biol Chem* 226: 497–509, 1957.
14. Garcia-Rua V, Otero MF, Lear PV, Rodriguez-Penas D, Feijoo-Bandin S, Noguera-Moreno T, Calaza M, Alvarez-Barredo M, Mosquera-Leal A, Parrington J, Brugada J, Portoles M, Rivera M, Gonzalez-Juanatey JR, and Lago F. Increased expression of fatty-acid and calcium metabolism genes in failing human heart. *PLoS One* 7: e37505, 2012.
15. Gouspillou G, Rouland R, Calmettes G, Deschodt-Arsac V, Franconi JM, Bourdel-Marchasson I, and Diolez P. Accurate determination of the oxidative phosphorylation affinity for ADP in isolated mitochondria. *PLoS One* 6: e20709, 2011.
16. Hauptmann N, Grimsby J, Shih JC, and Cadenas E. The metabolism of tyramine by monoamine oxidase A/B causes oxidative damage to mitochondrial DNA. *Arch Biochem Biophys* 335: 295–304, 1996.
17. Kane DA, Lin CT, Anderson EJ, Kwak HB, Cox JH, Brophy PM, Hickner RC, Neufer PD, and Cortright RN. Progesterone increases skeletal muscle mitochondrial H2O2 emission in nonmenopausal women. *Am J Physiol Endocrinol Metab* 300: E528–E535, 2011.
18. Koya T, Miyazaki T, Watanabe T, Shichiri M, Atsumi T, Kim-Kaneyama JR, and Miyazaki A. Salusin-beta accelerates inflammatory responses in vascular endothelial cells via NF-kappaB signaling in LDL receptor-deficient mice *in vivo* and HUVECs *in vitro*. *Am J Physiol Heart Circ Physiol* 303: H96–H105, 2012.
19. La Favor JD, Anderson EJ, Hickner RC, and Wingard CJ. Erectile dysfunction precedes coronary artery endothelial dysfunction in rats fed a high-fat, high-sucrose, Western pattern diet. *J Sex Med* 10: 694–703, 2013.
20. Larsson E, Mannervik B, and Raffalli-Mathieu F. Quantitative and selective polymerase chain reaction analysis of highly similar human alpha-class glutathione transferases. *Anal Biochem* 412: 96–101, 2011.
21. Li M, Liu JT, Pang XM, Han CJ, and Mao JJ. Epigallocatechin-3-gallate inhibits angiotensin II and interleukin-6-induced C-reactive protein production in macrophages. *Pharmacol Rep* 64: 912–918, 2012.
22. Mirzaei K, Hossein-nezhad A, Emamgholipour S, Ansar H, Khosrofar M, Tootee A, and Alatab S. An exonic peroxisome proliferator-activated receptor-gamma coactivator-1alpha variation may mediate the resting energy expenditure through a potential regulatory role on important gene expression in this pathway. *J Nutrigenet Nutrigenomics* 5: 59–71, 2012.
23. Paglia DE and Valentine WN. Studies on the quantitative and qualitative characterization of erythrocyte glutathione peroxidase. *J Lab Clin Med* 70: 158–169, 1967.
24. Perry CG, Kane DA, Lin CT, Kozy R, Cathey BL, Lark DS, Kane CL, Brophy PM, Gavin TP, Anderson EJ, and Neufer PD. Inhibiting myosin-ATPase reveals a dynamic range of mitochondrial respiratory control in skeletal muscle. *Biochem J* 437: 215–222, 2011.
25. Ramprasath T, Murugan PS, Kalaiarasan E, Gomathi P, Rathinavel A, and Selvam GS. Genetic association of Glutathione peroxidase-1 (GPx-1) and NAD(P)H:Quinone Oxidoreductase 1(NQO1) variants and their association of CAD in patients with type-2 diabetes. *Mol Cell Biochem* 361: 143–150, 2012.
26. Ruiz-Ferrer M, Torroglosa A, Nunez-Torres R, de Agustin JC, Antinolo G, and Borrego S. Expression of PROKR1 and PROKR2 in human enteric neural precursor cells and identification of sequence variants suggest a role in HSCR. *PLoS One* 6: e23475, 2011.
27. Rusai K, Prokai A, Szebeni B, Meszaros K, Fekete A, Szalay B, Vannay A, Degrell P, Muller V, Tulassay T, and Szabo AJ. Gender differences in serum and glucocorticoid regulated kinase-1 (SGK-1) expression during renal ischemia/reperfusion injury. *Cell Physiol Biochem* 27: 727–738, 2011.
28. Schults MA, Chiu RK, Nagle PW, Wilms LC, Kleinjans JC, van Schooten FJ, and Godschalk RW. Genetic polymorphisms in catalase and CYP1B1 determine DNA adduct formation by benzo(a)pyrene *ex vivo*. *Mutagenesis* 28: 181–185, 2013.
29. Senthil Kumar KJ, Liao JW, Xiao JH, Gokila Vani M, and Wang SY. Hepatoprotective effect of lucidone against alcohol-induced oxidative stress in human hepatic HepG2 cells through the up-regulation of HO-1/Nrf-2 antioxidant genes. *Toxicol In Vitro* 26: 700–708, 2012.
30. Stanley BA, Sivakumaran V, Shi S, McDonald I, Lloyd D, Watson WH, Aon MA, and Paolocci N. Thioredoxin

reductase-2 is essential for keeping low levels of H(2)O(2) emission from isolated heart mitochondria. *J Biol Chem* 286: 33669–33677, 2011.

31. Tietze F. Enzymic method for quantitative determination of nanogram amounts of total and oxidized glutathione: applications to mammalian blood and other tissues. *Anal Biochem* 27: 502–522, 1969.
32. Vanderlelie J, Gude N, and Perkins AV. Antioxidant gene expression in preeclamptic placentae: a preliminary investigation. *Placenta* 29: 519–522, 2008.
33. Zhang L, Bao Y, and Li J. Nuclear respiratory factor-1 is involved in mitochondrial dysfunction induced by benzo(a)pyrene in human bronchial epithelial cells. *Basic Clin Pharmacol Toxicol* 109: 115–122, 2011.